Functional Materials 13, No.1 (2006)

Structure influence on mechanical properties of Ti–W–B system nanocrystalline coatings

O.V.Sobol', S.N.Dub*, O.N.Grigor'ev**, A.A.Podtelezhnikov, A.N.Stetsenko

National Technical University "Kharkiv Polytechnical Institute",
21 Frunze St., 61002 Kharkiv, Ukraine
*V.Bakul' Institute for Superhard Materials, National Academy of Sciences of Ukraine, 2 Avtozavodskaya St., 04074 Kyiv, Ukraine
**I.Frantsevich Institute for Materials Science Problems, National Academy of Sciences of Ukraine, 3 Krzhyzhanovsky St., 03142 Kyiv, Ukraine

Received September 5, 2005

The effect of structure on nano-hardness and elastic modulus of Ti–W–B nanocrystalline coatings prepared by triode sputtering has been studied. The material structure state has been found to change from cluster-crystalline (at low sputtering potentials $U = 0.6$ to 1.0 kV) to preferentially oriented-crystalline (at $U > 2.2$ kV). The texture perfection improvement with increasing U results in increased hardness and elastic modulus of the condensates. The maximum values were attained at $U = 3.2$ kV and amounted $H = 19.9$ GPa and $E = 205$ GPa for the cubic phase and $H = 37.9$ GPa, $E = 389$ GPa for the hexagonal phase, respectively.

Исследовано влияние структуры нанокристаллических Ti–W–B покрытий, полученных триодным распылением, на их нанотвердость и модуль упругости. Выявлено изменение структурного состояния материала от кластерно-кристаллического при низких значениях распыляющего напряжения $U = 0{,}6...1{,}0$ кВ до преимущественно ориентированного-кристаллического при $U > 2{,}2$ кВ. Рост совершенства текстуры с увеличением U приводит к повышению твердости и модуля упругости конденсатов. Максимальные значения были достигнуты при $U = 3{,}2$ кВ и составляют для фазы с кубической решеткой: твердость $H = 19{,}9$ ГПа, модуль упругости $E = 205$ ГПа, а для фазы с гексагональной решеткой: $H = 37{,}9$ ГПа, $E = 389$ ГПа.

Among IV–VI group transitional metal diborides, it is just titanium diboride (TiB_2) that possesses the highest lattice stiffness [1] as is indicated by its both high hardness and melting temperature. Additionally, due its low density and high chemical stability, titanium diboride is among the most prospective materials to manufacture workpieces with high wear and heat stability. Nevertheless, strong directed covalent bonds and high stiffness level characteristic of TiB_2 phase result in low ductility and poor bending and tensile strengths which considerably restricts the application area of the ceramics. Therefore, presently, the ways to composite materials based on titanium diboride in combination with more ductile materials as the binders are being searched. One of the promising systems is the quasi-binary system TiB_2–W_2B_5, which may be described as a ceramic composite with W_2B_5 phase as the "more ductile" component. A substantial increase in the strength, hardness and cracking resistance have been found for hot-pressed Ti–W–B material as compared to single-phase materials — titanium boride and tungsten boride [2–4].

TiB_2–W_2B_5 is an eutectic type system with wide solubility range on the side of TiB_2 (solubility limit of W_2B_5 in TiB_2 attains 63 mol.%), while, according to quasi-binary equilibrium diagram, TiB_2 is practically insoluble in W_2B_5. This fact offers some prospects for strengthening the ceramics using heat treatments resulting in disintegration of supersaturated solid solutions obtained due to high temperature quenching [2].

As it was found experimentally, the transition metal nitrides, borides and carbides being in film state may demonstrate mechanical properties much exceeding the corresponding characteristics of bulks due to their structure peculiarities [5–8]. For example, TiB_2 boride coating wear resistance may be one decimal order higher than that of bulk analogs [8, 9]. In this connection, as a further step towards improving the mechanical properties of boride materials, the purpose of this work is to study the structure influence on mechanical characteristics of quasi-binary Ti–W–B system borides in film state.

The 2 to 2.5 μm thick coatings were obtained using a triode sputtering system [10]. The potential U = 600 to 3200 V was applied to the target. The ion current varied from 100 to 250 mA. In the first case, the condensation rate (v) was 0.11 nm/s, while in the second case, 0.25 nm/s. The target-to-substrate distance was 7.5 cm. The working gas was pure argon (99.7 %). The working gas pressure at the condensation did not exceed 0.4 Pa. To purify additionally the working gas, titanium was sputtered near the input zone. The preliminary ion cleaning was carried out using negative potential 700 V applied to the substrate. The substrate heating with the coating did not exceed 530°C. As the substrate materials, polished (111) silicon single crystal of 350–360 μm thickness, 500–520 μm thick glass ceramics, and over 1mm thick tantalum were used. The target was a hot-pressed disk of 80 vol.% WB_5–20 vol.% TiB_2 of 105 mm diameter and 5 mm thickness. A difference between triode sputtering method and ion-plasma magnetron sputtering widely used today consists in the uniformity of target sputtering and absence of any substantial planarity disturbance during sputtering. Thus, at texture formation in condensed films, the texture axis [00.1] inclination angle to the film normal did not exceed 2...3°.

The phase composition and structure was analyzed using a DRON-3 diffractometer in

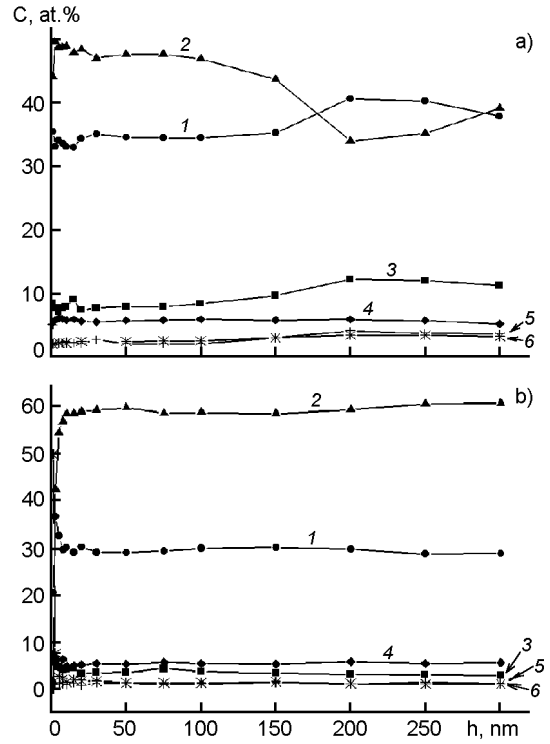

Fig. 1. Elemental atomic concentration (C) in the film with (a) cubic phase (W,Ti)B (v = 0.11 nm/s, U = 3200 V), and (b) hexagonal phase $(W,Ti)B_2$ (v = 0.25 nm/s, U = 3200 V) vs. the etched surface layer thickness (h). Atomic distributions: *1*, W; *2*, B; *3*, C; *4*, Ti; *5*, O; *6*, N.

Ni-filtered radiation of Cu anode, and DRON-2 in Mn-filtered radiation of Fe anode in θ–2θ geometry with Bragg-Brentano focusing. Registration both in discrete and continuous regimes was applied. At continuous registration on diagram tape, its motion velocity was 12 mm/min at goniometer angular velocity 2 deg/min. At discrete registration, a scan step was $\Delta(2\theta)$ = 0.01 to 0.05° with exposure time of 40 to 100 s per point. The condensate density was determined using X-ray reflectivity method with incident angles near total reflection angle [11]. The elemental composition was analyzed using a RIBER LAS-2000 Auger spectrometer in micro-profiling and scanning microprobe spectrometry modes. To remove adsorbed impurities from the sample surface as well as during micro-profiling, Ar^+ ion etching at 4 keV energy was used. The etch spot diameter was 2 mm, the etching rate 5 nm/s. All the measurements were carried out in analytic chamber under 10^{-5}–10^{-6} Pa vacuum using a standard technique. The hardness (H) and elastic

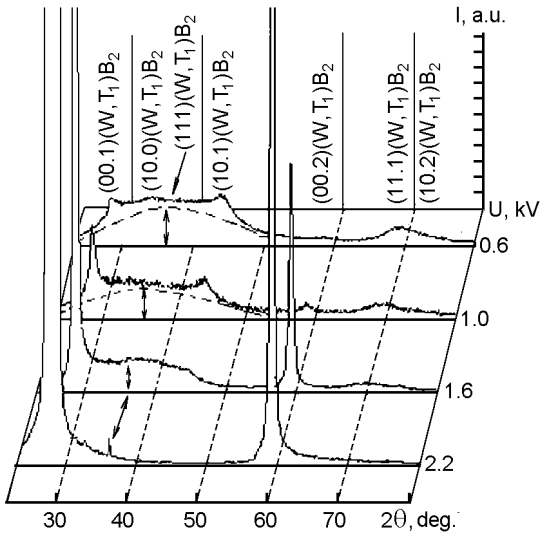

Fig. 2. Diffraction pattern fragments for film samples obtained by triode sputtering at different sputter voltages (kV): *1*, 0.6; *2*, 1; *3*, 1.4; *4*, 2.2 ($Cu–K_\alpha$ radiation).

modulus (E) were measured using Nano Indenter II MTS System with diamond indenter in the shaped as a three-face pyramid with apex angle 65.3° (Berkovich indenter). For mechanical examination of thin films, highly local methods are required, for example, micro-hardness tests. To exclude the substrate effect on testing results, it is necessary that indention depth would at least ten times less than film thickness. Such investigations become possible using nano-indentation method, with hardness being determined by indention depth and elastic modulus being calculated from the indenter loading-unloading curves [15].

The film phase composition analysis has shown that, except for supersaturated solid solution $(Ti,W)B_2$ (hexagonal AlB_2 crystal lattice, space group $P6/mmm$) characteristic of ion-plasma quasi-binary TiB_2–W_2B_5 condensates [12], at low current (100 mA) and condensation rate (0.11 nm/s), the coatings containing (Ti,W)B phase with NaCl type cubic crystal lattice are formed. Moreover, the coatings were almost single-phase (i.e., there were none of lines in the diffraction patterns, except for diffraction lines (111), (200), (220), (311), (222) and so on characteristic of the NaCl type cubic lattice). Comparative analysis of diffraction patterns has shown that with increasing sputtering potential, the coating crystallite orientation changed from perpendicular to growth plane preferential direction [111] to [100] one. Moreover, as increases U from 1 to 3.2 kV,

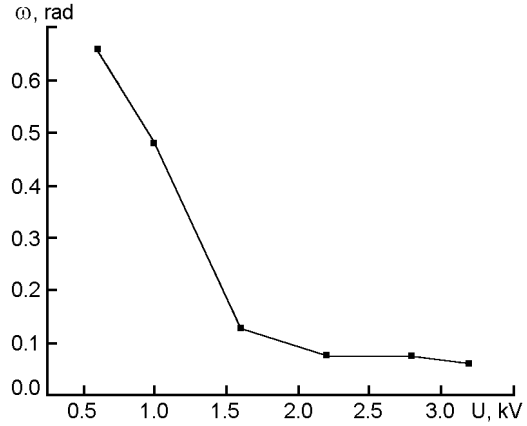

Fig. 3. Structure perfection defined by rocking curve FWHM, ω, vs. sputter potential, U.

the diffraction lines shift towards extended angles corresponding to lattice parameter decrease from 0.426 to 0.4235 nm. X-ray tensometric measurements have shown [13] that in (W,Ti)B coatings with cubic crystal lattice, tensile macro-strain of about 0.8 to 1 % appears.

Studying the elemental composition depth distribution across the coatings with cubic crystal lattice, the main constituent ratio (tungsten, titanium and boron) was found to vary as compared to the pre-calculated value (in the target, metal-to-boron ratio is 1:2 according to the composition), Fig. 1a. In the coating, a relative decrease of boron atomic concentration is observed, the most intense at the initial deposition stages (i.e. in the deper layers of the film). In this case, the metal/boron atomic ratio became close to a unity. The relative decrease of boron atomic amount in the coating correlates with increase of dissolved carbon impurity concentration (Fig. 1a, curves *2*, *3*).

As the condensation rate increases to 0.25 nm/s, the supersaturated solid solution $(W,Ti)B_2$ with hexagonal crystal lattice is observed to be formed in the films. The comparison of the results for different sputtering energies has shown that the sputtering potential increase from 0.6 to 3.2 kV results in texture development with the preferential orientation axis [00.1] perpendicular to the growing film surface.

The expansion of experimental diffraction profiles obtained in the angular range 2θ = 23...57° into the constituent lines using Cauchy approximation function $(1 + \alpha_1 x^2)^{-1}$ (α_1 — parametric coefficient) showed a "halo" with maximum corresponding to d = 0.231 nm for samples prepared at U = 0.6 to 1.6 kV (in Fig. 2, the diffraction line portion corre-

sponding to cluster component is shown by a dashed line, and its maximum position is indicated by an arrow). With increasing sputter energy, the fraction of cluster component in the whole condensate volume decreases and results in lowered intensity of characteristic "halo" (Fig. 2, curves 1–3). Simultaneously with decreasing intensity of diffraction lines from cluster component, the narrow lines from NaCl type cubic crystal lattice are observed. At relatively low [00.1] texture degree of $(W,Ti)B_2$ crystallites (U = 1.6 kV), a small diffraction peak with position corresponding to (111) line of cubic (W,Ti)B phase is observed against the halo-like line background (Fig. 2, curve *3*). Increasing the texture degree of solid solution $(W,Ti)B_2$ crystallites with hexagonal (00.1) plane preferential orientation parallel to the growth surface at increasing U is followed by (W,Ti)B crystallite formation with cubic lattice and preferential orientation (111). In X-ray diffraction spectra, two reflection orders from texture plane are revealed (Fig. 2, curve *4*, texture plane (111) is indicated by an arrow) and all the reflections from the planes inclined to the texture plane at corresponding angles for cubic crystal lattice. The cause of texture occurring at the cubic phase crystallization could be the coherently bonded growth (epitaxy) of (W,Ti)B crystallites under their formation on grain boundaries of $(W,Ti)B_2$ solid solution.

The estimation of [00.1] texture perfection of $(W,Ti)B_2$ solid solution crystallites (with hexagonal lattice) by (00.2) reflection rocking curve FWHM variation has shown (Fig. 3) an abrupt drop on U dependence in the range 1.0–1.6 kV. It is in this range, the transition from bistructural cluster-crystalline state to crystalline one takes place (Fig. 2).

Elemental composition analysis of coatings obtained at the rate v = 0.25 nm/s shows rather uniform element distribution in depth with main element ratios close to the target ones at relatively high condensation rate (Fig. 1b). The substructure characteristic study performed by approximating the profiles of X-ray diffraction lines [13] for two reflection orders of (00.1) texture line of $(W,Ti)B_2$ and (111) for (W,Ti)B with cubic lattice has shown that the average crystallite size in the texture axis direction [00.1] in hexagonal $(W,Ti)B_2$ exceeds 50 nm, while in (W,Ti)B phase with cubic lattice, that in the direction of texture axis [111] is substantially less (23 nm).

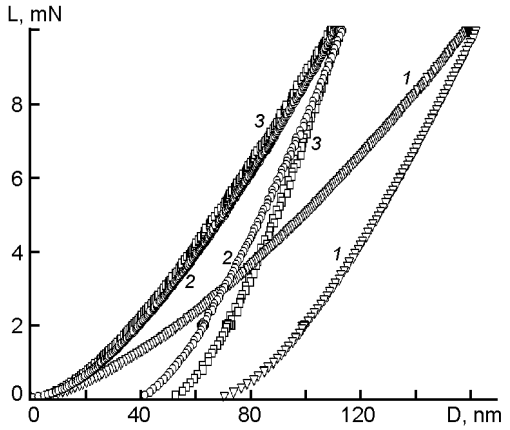

Fig. 4. Load-displacement curves for Ti–W–B films obtained at U = 3.2 kV with cubic (*1*) and hexagonal (*2*) crystalline lattices, and for the bulk W_2B_5 reference with hexagonal lattice (*3*).

The specific shape of typical loading-displacement curves shown in Fig. 4 for film samples and bulk reference W_2B_5 indicates no peculiarities in the curves which would result from breaking or plastic yield of the film material under indentation. Therefore, the observed differences between the loading-displacement curves for the films with cubic and hexagonal crystal lattices are connected with different inherent straining mechanisms. The strained layer depth under nano-indentation was 110–190 nm that is one decimal order larger than compositionally inhomogeneous surface layer. In the Table, the results of nano-indentation for films with cubic and hexagonal lattices are summarized. As it is seen from the Table, there is a principal difference in mechanical properties between the $(W,Ti)B_2$ films with hexagonal lattice and (W,Ti)B films with cubic one. Elastic modulus and hardness of cubic lattice films are substantially lower than those for the hexagonal lattice ones.

It should be noted that for the samples obtained at higher sputtering rate v = 0.25 nm/s, the structure changed from cluster-crystalline (in the range U = 0.6–1.6 kV, Fig. 2, curve *1–3*) to two-phase crystalline one with phase volume ratio h-$(W,Ti)B_2$/c-(W,Ti)B ≈ 9:1 (at U = 2.2 kV, Fig. 2, curve *4*), and further, to strongly textured crystalline structure with ratio h-$(W,Ti)B_2$/c-(W,Ti)B > 20 at U = 3.2 kV. It is seen that for this film series, the crystallinity degree increase results in a higher hardness, while elastic modulus drops a little in the sample obtained at U = 2.2 kV with substantial concentration of cubic phase. The main cause of elastic modulus decrease in two-

Table. Nano-indentation data for triode sputtered films with cubic and hexagonal crystalline lattices under indenter load 10 mN

Sputter potential U, kV	Condensation rate v, nm/s	Lattice type	Elastic modulus E, GPa	Hardness H, GPa
0.6	0.25	Hexagonal	291	27.3
1.6	0.25	Hexagonal	373	34.1
2.2	0.25	Hexagonal + cubic	317	37.9
3.2	0.25	Hexagonal	389	37.0
1.0	0.11	Cubic + hexagonal	194	15.6
2.2	0.11	Cubic	162	13.9
3.2	0.11	Cubic	206	19.9
W_2B_5-bulk		Hexagonal	496	32.4

phase samples could be micro-discontinuities occurring during the crystallization at grain boundaries with cubic phase being formed in the boundary area. A confirmation of this is the relative density decrease of the condensate obtained at $U = 2.2$ kV by a factor 0.78 as compared to theoretical density for the specific target composition ($\rho \approx 11$ g/cm^3). For the second sample series with the main cubic phase obtained at the rate $v = 0.11$ nm/s, a substantial decrease of hardness and elasticity modulus is observed. Nevertheless, in this case as well, the (100) texture in the samples obtained at $U = 3.2$ kV results in higher mechanical characteristics.

Consideration of the results obtained allows to define three key points which could characterize the peculiarities of structure state and mechanical characteristics of triode-sputtered films in quasi-binary W_2B_5–TiB_2 system. The first point is the substantial effect of the condensation rate on elemental and phase composition. The second one is the stability of the phase being not corresponding to equilibrium diagram for the system. The third is the formation of bi-structure cluster/crystalline coating and the effect of its perfection degree on mechanical characteristics.

A more detailed consideration of the first point shows that, in contrast to high condensation rate conditions when the metal/boron atomic ratio in the deposited coating remains close to stoichiometric MeB_2 value, at low condensation rate, the relative boron content becomes lower. The process is seen to be similar to effect observed in [14] for magnetron sputtering at tungsten carbide deposition rates close to those used in our work. It is just the relatively lowered atomic sticking coefficient for W–C(B) system as compared to, for example, Ti–C(B), as well as preferential resputtering the light elements from the film growth surface with back-scattered neutral argon atoms that are considered as the causes of the light component relative content decrease in tungsten based coating. It should be noted that under analogous regimes of TiC coating deposition, the stronger titanium-carbon bond results in conservation of the atomic ratio close to the stoichiometric one [14].

One of the main causes of metastable cubic structure occurrence at low deposition rates seems to consist in more effective capture of light impurities (O, N, C) and a complex phase $(W,Ti)B_{0.7...1.2}(C,O,N)_{0.3...0.2}$ formation with lack of metal atoms. Weakening of the metal bonds seems to be a cause of hardness and elastic modulus decrease in the coatings with cubic lattice. When discussing the causes of lowered elastic modulus in hexagonal $(W,Ti)B_2$ based coatings in comparing with bulk values ($E \approx 500$ GPa), inter-crystallite boundary specific density increase with decreasing crystallite size to nanoscale values as well as metal/boron binding weakening due to decreased titanium concentration should be taken into consideration. Non-equilibrium boundaries in nano-materials form an effective sink for different types of defects including the dissolved impurity atoms. Considering the structure of boundary defects, it should be noted that in nano-crystalline materials, the intergrain boundary width is about 0.5 to 3 nm, according to various estimations [16, 17]. The non-equilibrium grain boundaries contain a lot of dislocations, and there are non-compensated disclinations in grain joints. Dislocations and disclinations create the long-range stress fields

concentrated near grain boundaries and triple joints and are responsible for the grain boundary excess energy.

The material volume increase due to the defects would result in increased least-square atomic shift amplitude. To estimate the atomic shifts in the direction perpendicular to grain boundary, an empiric formula, $\Delta \approx a \cdot \varepsilon$ [18] can be used, where a is the crystal lattice parameter, and ε, the lattice strain. The value $\Delta = 0.01$ nm typical of nanocrystals for lattice parameter value 0.31 nm corresponds to 3 % lattice strain. In this connection, the strain values 1 % obtained in this work seem to be reasonable and correspond to the proposed model. The observed increased boundary energy is followed by atomic vibration amplitude in lattice sites which promotes the material "plasticization". The estimation of boundary state effect on nano-material elasticity made in [19] has shown that for the boundary width 1 nm, the elastic modulus E may be lower by a factor of 6 than that for bulk state, while the relative shear modulus G decrease may approach a factor 8. In this connection, the obtained relatively low modulus E value indicates a high contribution of boundary properties into formation of integral mechanical properties of nano-condensates in quasi-binary W_2B_5–TiB_2 system.

From the data presented, it is seen that at relatively low ion bombardment energies, the coatings of "cluster/crystallite" type are formed, that results in a drastic decrease of elastic modulus and hardness. Increasing the average energy of deposited particles at the sputter potential increase promotes crystallization process which mainly causes the hardness increase. The elastic modulus increase seems to be influenced mainly by the coating density which is known to rise in diborides with deposited particle average energy [20]. In this work, this results in the highest elastic modulus value attained at sputtering at the highest energy of 3.2 kV.

The material plasticity improvement is promoted by cluster component appearing under relatively low sputter potential ($U = 0.6$–1.6 kV). The results obtained show that under sputter potentials (0.6, 1.0 and 1.6 kV), the width of the broadened reflection at $2\theta = 37°$ in X-ray diffraction patterns shown in Fig. 2 (curves *1, 2, 3*) remains practically constant at 14°, which corresponds to coherence length of 0.67 nm, according to Selyakov-Sherrer formula [13]. If the lattice parameter 0.425 nm typical of

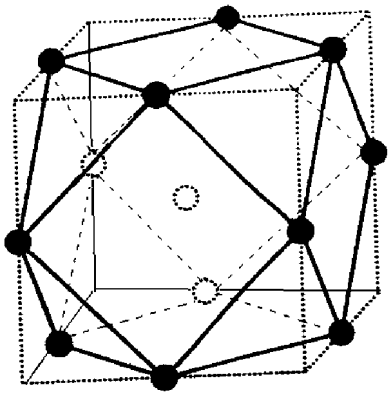

Fig. 5. Scheme of 13-atomic fcc cluster of 14-hedron shape.

the most close packed cubic lattice with 4 metal atoms per unit is used to estimate the number of atoms in the cluster, the obtained cluster size corresponds to an aggregate containing 13 metal atoms, while boron atoms (exceeding significantly in size the free volume of octahedral interstitials) may be partially driven out to cluster boundaries, thus stimulating their stability and forming the stable bonds between the clusters.

It is well known [22–24] that for 3D-complexes of less than 300 metal atoms in a cluster, several magic structure numbers exist which correspond to the most close occupancy. For the structure range under consideration, the closest packed structures (packing coefficient 0.74) are icosahedral (packing coefficient 0.78) as well as fcc and hcp (packing coefficient 0.74). For all these structures, the first most stable cluster is an aggregate containing 13 atoms (1 in the center, and 12 in the first coordination sphere). In the following coordination spheres, there are some differences. For example, in fcc based structures, a row of stable atomic formations represents a sequence 13, 55, 147, 309, while in hcp, this is 13, 57, 153, 321. The minimum volume of fcc based cluster represents a 14-face polyhedron containing 13 atoms shown in Fig. 5. A visual representation of such 14-hedron is obtained by shifting the metal site atomic positions by a half of body diagonal leading to positioning one of them in the lattice center (Fig. 5). Such a structure named a cuboctahedron shows a high thermodynamic stability [21].

As it is seen from Fig. 2, the films contain, along with cluster component, nanocrystalline inclusions with average crystallite size from 4 nm (in the films obtained at

$U = 0.6$ kV) to 12 nm (in the films produced at $U = 1.6$ kV). Such bi-structural state corresponds to the classic scheme "plastic matrix — solid inclusion", which results in high mechanical properties at plastic binding component content less than 15 vol. % [25].

Thus, at a low condensation rate (0.11 nm/s), the formation of complex composition phase $(W,Ti)B_{0.7...1.2}(C,O,N)_{0.3...0.2}$ with cubic lattice has been revealed. It was found that the sputtering potential increase up to 3.2 kV results in formation of preferentially oriented crystallites with [00.1] axis perpendicular to the growth surface. Increased condensate hardness and elastic modulus are consequences of the structure perfection improvement. High condensation rates result in formation of boride coatings with low gaseous impurity concentrations (C, N, O) and stimulate the formation of a phase with hexagonal lattice of AlB_2 type. The change of material structure from cluster-crystalline state at low sputter potentials ($U = 0.6$ to 1.0 kV) to textured crystalline one at $U > 2.2$ kV has been revealed. The maximum hardness value 37.9 GPa was attained for the samples with strong texture [00.1] obtained at the highest $U = 3.2$ kV, elasticity modulus being $E = 389$ GPa.

References

1. G.V.Samsonov, T.I.Serebryakova, V.A.Neronova, Borides, Atomizdat, Moscow (1975) [in Russian].
2. L.I.Gladkikh, O.N.Grigorev, O.V.Sobol' et al., *Prob.Atomic Sci.Tech.*, **82**, 139 (2002).
3. A.Pohl, P.Kizler, R.Telle, F.Alinger, *Z.Metallkd.*, **85**, 658 (1994).
4. C.Schmalzried, R.Telle, B.Freitag, W.Mader, *Z.Metallkd.*, **92**, 1197 (2001).
5. S.Veprek, A.S.Argon, *Surf.Coat.Technol.*, **146–147**, 175 (2001).
6. J.Musil, *Surf.Coat.Technol.*, **125**, 322 (2000).
7. M.Berger, E.Coronel, E.Olsson, *Surf.Coat.Technol.*, **185**, 240 (2004).
8. M.Berger, L.Karlsson, M.Larsson, S.Hogmark, *Thin Solid Films*, **401**, 179 (2001).
9. M.Berger, M.Larsson, S.Hogmark, *Surf.Coat.Technol.*, **124**, 253 (2000).
10. O.V.Sobol', E.A.Sobol', A.A.Podtelezhnikov, S.T.Roshchenko, *Functional Materials*, **7**, 305 (2000).
11. A.V.Vinogradov, I.A.Brytov, A.Ya.Grudsky et al., X-Ray Mirror Optics, Mashinostroyeniye, Leningrad (1989) [in Russian].
12. O.V.Sobol', A.T.Pugachov, A.N.Stetsenko, *Vestnik VSTU*, **15**, 18 (2004).
13. I.C.Noyan, J.B.Cohen, Residual Stress Measured by Diffraction and Interpretation, MRE Springer, New York (1987).
14. J.-P.Palmquist, Zs.Czigany, M.Oden et al., *Thin Solid Films*, **444**, 29 (2003).
15. W.C.Oliver, G.M.Pharr, *J.Mater.Res.*, **7**, 1564 (1992).
16. W.Losh, P.M.Jardim, *Scripta Mater.*, **38**, 1857 (1998).
17. X.Zhu, R.Birringer, U.Herr, H.Gleiter, *Phys.Rev.*, **35**, 9085 (1987).
18. R.Z.Valiyev, I.V.Aleksandrov, Nano-Structural Materials Obtained Using Intensive Plastic Deformation, Logos, Moscow (2000) [in Russian].
19. A.I.Gusev, A.A.Rempel, Nano-Crystalline Materials, Fiz. -Mat. Lit., Moscow (2001) [in Russian].
20. J.Ye, S.Ulrich, K.Sell et al., *Surf.Coat.Technol.*, **174–175**, 959 (2003).
21. C.P.Pool, F.J.Owens, Introduction to Nanotechnology, Wiley Interscience, New York (2003).
22. Yu.I.Petrov, Physics of Small Particles, Nauka, Moscow (1982) [in Russian].
23. V.A.Polukhin, Nanostructure and Precursor Modeling, Ural Div. of RAS, Ekaterinburg (2004) [in Russian].
24. A.P.Shpak, O.V.Sobol', Yu.A.Kunitsky, P.G.Cheremskoy, Self-Organizing of Low-Dimensional Systems, IMPh NASU, Kyiv (2005) [in Russian].
25. J.Patscheider, *MRS Bull.*, **28(3)**, 180 (2003).

Вплив структурного стану на механічні властивості нанокристалічних покриттів системи Ti–W–B

О.В.Соболь, С.М.Дуб, О.М.Григор'єв, А.О.Подтележніков, О.М.Стеценко

Досліджено вплив структури нанокристалічних Ti–W–B іонно-плазмових (тріодна схема) покриттів на їх нанотвердість та модуль пружності. Виявлено зміни структурного стану матеріалу від кластерно-кристалічного при низьких значеннях U = 0,6...1,0 кВ до переважно орієнтованого кристалічного при U > 2,2 кВ. Зростання досконалості текстури зі збільшенням U призводить до зростання твердості та модулю пружності конденсатів. Максимальні значення досягнуто при U = 3,2 кВ і складають для фази з кубічною граткою: твердість H = 19,9 ГПа, модуль пружності E = 205 ГПа, а для фази з гексагональною граткою: H = 37,9 ГПа, E = 389 ГПа.